Optical Beamforming Concepts for Wide-Swath Synthetic Aperture Radar Systems

J. Ydreborg[1]*, S. Huber[1], and G. Krieger[1]

[1]German Aerospace Centre (DLR), Germany *josef.ydreborg@dlr.de

Publisher url: `https://ieeexplore.ieee.org/abstract/document/10221395`

Abstract— High-resolution wide-swath (HRWS) imaging using scan-on-receive (SCORE) synthetic aperture radar (SAR) with one or multiple simultaneous beams is being heavily investigated using digital beamforming paradigms. However, a contender is analogue beamforming using photonics. In this work, the feasibility of photonics enhanced beamforming in SAR systems in higher frequency bands and bandwidths is investigated using a state-of-the-art SAR system as a comparison. The most common performance indicators are derived and an example SAR system is devised, with a discussion on potential antenna configurations. The integrated microwave photonics (IMWP) platforms available and most suited to SAR systems is discussed, including architectures and materials. Additionally, an investigation into system noise and dynamic range performance reveals a number of essential challenges that need to be addressed, including the reduction of losses an thereby the required number of semiconductor optical amplifiers (SOA) and the noise performance of the laser(s). The reconfiguration speed of beamforming phase shifters and true-time delay (TTD) elements are essential for SCORE operation with a large number of beams, which limits the viable materials used for these elements. The current state of IMWP indicate that these advanced systems with many beams and channels is very difficult to realize for SAR and implementations in simpler systems are more viable. However, the rapid development of IMWP indicate that these beamforming systems will soon be viable for SAR.

1. INTRODUCTION

Imaging using conventional synthetic aperture radar (SAR) is a mature technology that is used for a wide variety of remote sensing applications. However, the performance of conventional SAR is limited by the minimum antenna area constraint, forcing a trade-off between swath width and azimuth resolution [1][2]. High-resolution wide-swath (HRWS) SAR exploiting the Scan-On-Receive (SCORE) technique, represents an approach to map very wide swaths on ground and, at the same time, improve the noise equivalent sigma zero (NESZ), suppress range ambiguities, maximize available gain, while also reducing antenna pattern edge losses. The idea, involving steering a beam in line with the direction of the echo, originated with Blythe [3] and was later developed further by Kare [4] and Suess and Wiesbeck [5], introducing the use of reflector antenna and digital beamforming, respectively. These techniques have subsequently further developed and extended in later works. Examples are dispersive SCORE, multi-beam SCORE, and Staggered SAR which make extensive use of a digital beamforming (DBF) paradigm [6][7][8][9]. However, recent developments in photonic technologies have made photonic beamforming (PBF) a potential analogue contender to DBF methods [10][11][12]. Indeed, many features of optical beamforming networks (OBFN), such as small relative bandwidth, near frequency agnostic operation in SAR frequency bands, low power consumption and low computational requirements, make their implementation in SAR systems an enticing prospect [10][13]. Additionally, recent developments in integrated microwave photonics (IMWP) technologies have opened up opportunities for smaller form factors, more complex systems and more temperature stable and predictable performance than bulk fibre-optic systems can provide [14][15][16]. This makes IMWP-based beamforming potentially a key technology in enabling swarm, constellation and cubesat SAR systems in low earth orbit due to its excellent size, weight and power (SWaP) properties. Additionally, recent research and trends indicate a rapid expansion of the number of components housed per chip, as well as a performance increase and manufacturing cost reductions of photonic integrated circuits (PIC) in the near future in a phenomenon similar to Moore's law [17][18][19].

This paper investigates the feasibility of photonic networks to implement a state-of-the art SAR with SCORE as a benchmark for potential architectures, leading to a number of requirements such as noise equivalent sigma zero (NESZ), ambiguity-to-signal ratio (ASR), and dynamic range. Inserting an OBFN in the SAR receive chain impacts the performance of the system in a number of different ways, including noise performance, dynamic range, pointing errors, and beamforming weights reconfiguration speed. The paper assumes the implementations using integrated microwave photonics (IMWP) in the optical communication C-band carrier wavelength (1530–1565 nm). The most prevalent modulation strategy is external intensity modulation direct-detection (IMDD) and as such the paper is limited to this paradigm. Furthermore, the investigation focuses on elevation beamforming and the gaps present when employing multiple simultaneous SCORE beams will not be dealt with in this investigation [20].

The outline is as follows. Section 2 presents modern SAR requirements and an example system as a basis for discussion, while also discussing the two most prominent antenna architectures associated with SCORE. Section 3 presents a number of architectures for OBFNs and the potential IMWP materials and platforms that are most suited to these architectures, bearing in mind the requirements in section 2. Section 4 further discusses challenges in the system performance and their impact on noise and dynamic range. Finally, section 5 wraps up the paper with a discussion and conclusion.

2. STATE-OF-THE-ART SAR

2.1. SAR requirements and parameters

Table 1: Imaging requirements for a modern SCORE SAR example system.

Requirement	Value
Frequency	X band or Ka band
Noise Equivalent Sigma Zero	≤ -27 dB
Ambiguity-to-Signal Ratio	≤ -27 dB
Dynamic Range	≥ 32 dB
Ground Resolution	≤ 1.7 x 1.7 m (2.9 m^2)
Beamforming Weights Accuracy	ampl. $\leq 0.4\%$, phase $\leq 1.4°$

The requirements placed on a modern SAR system implementing SCORE is listed in Table 1. As the prime benefits of photonics lie in the wide bandwidth and high RF operating frequency, the focus will lie on the X band and Ka band. The NESZ is derived from the expected scattering statistics of common ground targets as listed in Table 2, which list the weakest and strongest reflectivities for these targets. Given a imaging use case with varied ground targets, the weakest reflections come from asphalt, concrete and roads in the X band case, while wet snow is the weakest scatterer in the Ka band case [21]. This is a worst case scenario, since the beam generally covers a large area and exhibit larger reflectivity, especially in the higher frequency cases. For simplicity, the ambiguity-to-signal ratio (ASR) matches the requirement for the NESZ, but here the SAR mode and beamforming design primarily impact the results. In terms of the SCORE mode, range ambiguities are already more suppressed than a conventional SAR due to the receive pencil beam. However, a larger number of active elements in the antenna array would enable the system to place dedicated nulls at the angular location of ambiguities without compromising the SCORE operation [22]. The number of active channels achievable in current PIC technology, will be discussed later. The required dynamic range is tightly connected with the variation in reflectivity of ground targets, which show a span of approximately 32 dB and 30 dB for X band and Ka band, see Table 2. Additionally, the dynamic range requirement is impacted by the difference between the near and far ranges of the swath and the transmit antenna pattern, in the order of about 1-4 dB [2]. This can be mitigated using phase spoiling in transmit given enough active transmit elements [23]. The required resolution for a modern SAR system operating at X band or above would need to surpass or match the resolution of systems like TerraSAR-X and TanDEM-X while achieving a wider swath width [24]. Therefore, the ground resolution goal in Table 1 are set to less than the spotlight mode resolution of 1.7 x 1.7 metres. The comparison of accuracy as pertaining to beamforming weights becomes somewhat arbitrary given that DBF functionally does not have this restriction, while an analogue solution like PBF is affected by this phenomenon. Nonetheless, a resolution corresponding to a 8-bit attenuator and phase shifter (PS) accuracy has been given for discussion purposes.

In Table 3, the parameters for a single beam SCORE SAR system are detailed. Fairly standard

Table 2: Average ground reflectivity at 30° incidence angle by frequency band and ground type [21]. Considers HH and VV polarisations rounded to whole dBs.

Frequency	Target Type	Min Reflectivity	Max Reflectivity
X-band	Asphalt and Concrete	-27 dB	-10 dB
	Soil and Rock	-19 dB	4 dB
	Snow	-16 dB	-5 dB
	Trees and Vegetation	-19 dB	1 dB
Ka-band	Asphalt and Concrete	-17 dB	-3 dB
	Soil and Rock	-21 dB	-3 dB
	Snow	-23 dB	7 dB
	Trees and Vegetation	-16 dB	0 dB

orbit height, pulse repetition frequency (PRF) and duty cycle are assumed. The bandwidth chosen is restricted by the maximum frequency allocation permitted by ITU radio regulations at Ka-band (35500-36000 MHz) [25]. The available bandwidth at X band reaches 1200 MHz (9200-10400 MHz), but for this broader discussion the bandwidth will be limited to 500 MHz. This results in a maximum range resolution of approximately 0.62 m. The azimuth resolution is restricted to about 1.30 m due to the PRF limiting the antenna length, which could be improved using innovative multi-channel azimuth beamforming techniques [6]. The range of incidence angles include the 30° angle used in Table 2 and achieve an approximately 40 km swath width using a single SCORE beam (timing diagram in Fig. 1). If a wider swath without loss of azimuth resolution is desired additional simultaneous SCORE beams can be employed. In order to ensure a uniform intensity across the swath 115 SCORE beams are used to scan the swath on receive. This is a very high number of pointing directions, which may have to be reduced due to current PBF hardware limitations. The shortest beam dwell time is the first (near range) beam and lasts for 0.99 µs in this case.

Parameter	Value
Orbit Height	500 km
Pulse Repetition Frequency (PRF)	6 kHz
Duty Cycle	9% (15 µs)
Bandwidth	500 MHz
Range Resolution	0.62 m
Azimuth Resolution	1.30 m
Start Incidence Angle	26.2°
Stop Incidence Angle	30.2°
Swath Width	40 km
No. SCORE Beams	115
Dwell Time of First SCORE Beam	990 ns

Table 3: Parameters for an example modern SCORE SAR system.

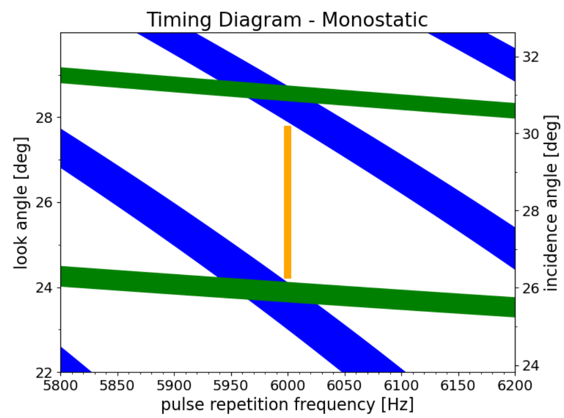

Figure 1: Timing diagram for SCORE SAR system (blue: transmit events, green: nadir echo, yellow: swath).

2.2. SAR antenna configuration

The type of antenna configuration employed impacts the beamforming network used and therefore the potential suitability of PBF. For SCORE SAR there are two main configurations envisioned; planar phased array (PA) antennas and phased array-fed reflector (PAFR) antennas. From the pure SAR perspective, the PA require involvement of all antenna elements to create a SCORE beam resulting in higher sensitivity to amplitude and phase errors and must therefore employ a stricter calibration strategy [26]. For the same task, a PAFR antenna only requires a single element for each beam, if placed at the focal point, and a small number if the feed array is slightly out of focus. This property of PAFRs enables the blass matrix architecture to be used with low to no overlap of active elements for each beam and thus reducing the BFN losses [4][27]. However, due to this property the PAFR is more sensitive to antenna element failures [28]. Additionally, thermo-elastic deformations of the reflector impact the pointing stability and radiometric performance of the PAFR system. The beamwidth of a PA is tightly connected to the number of elements employed, driving up the requirement for a large number of feeds to enable the SCORE beamforming mode with a large accessible ground area. The number of elements needed for a certain PA pencil beamwidth is governed by [27]

$$N_{\mathrm{el}} = \frac{\lambda}{\sin(\theta_{\text{-3dB}})\, d}, \tag{1}$$

where λ is the RF wavelength, $\theta_{\text{-3dB}}$ is the 3 dB beamwidth, and d is the element separation. Using the parameters of our example system in Table 3 and an example pencil beamwidth of 0.80°and element separation of 0.65 wavelengths, we can conclude that 111 PA antenna elements would be required. The current state of PIC technology preclude the implementation of that many channels, without using RF combining networks to reduce the number of channels before E/O conversion. One could also increase the antenna element separation with a narrower accessible ground area or widen the beamwidth at the expense of reduced gain. A such, the near-future suitability of OBFNs seem to be better in PAFRs due to the lower number of feed elements required and less extensive pattern weighting [27]. Further research is required to compare the use of OBFNs in PAFR and PAs with sub-arrays. Additionally, the employment of OBFNs using wavelength division multiplexing (WDM) strategies for separating multiple beams could be beneficial for the PA configuration.

3. IMWP PLATFORM

3.1. Photonic Beamforming Architectures

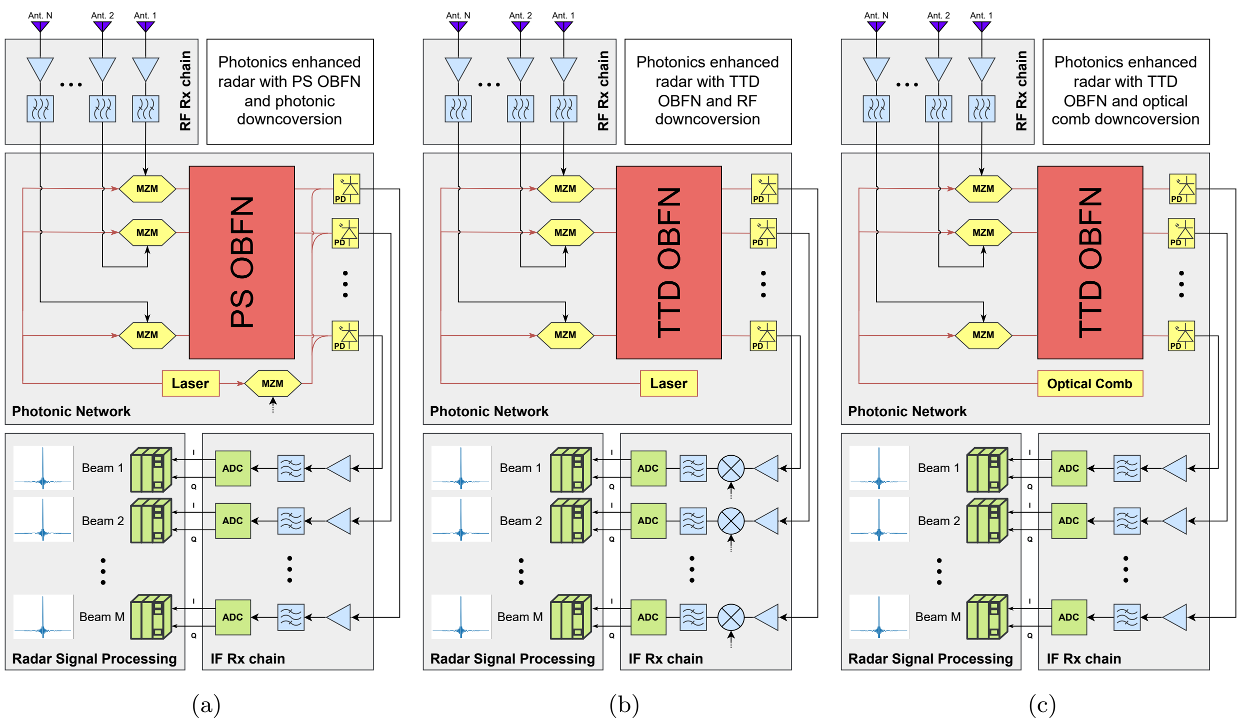

Figure 2: Simplified SAR receive chain including a) an OBFN employing phase shifters and photonic downconversion, b) an OBFN employing TTD and RF downconversion and c) an OBFN employing TTD and optical comb downconversion.

There are a number of potential beamforming architectures that could be used to construct an OBFN. Fig. 2a illustrates a generalized system employing a PS based OBFN where the received RF signals are modulated on an optical carrier and processed using photonics, including beamforming and downconversion. Since phase shifting affects both the carrier and the modulated signal, the carrier must be suppressed and re-inserted before photodetection in order for the phase shift to be seen in the RF domain [29]. It is convenient to combine this re-insertion with a photonic downconversion, performed via modulating the carrier with a local oscillator to reduce the beat frequency in the photodiode. The carrier suppression and re-insertion requirement is not present in a true time delay (TTD) system, as depicted in Figure 2b, where the downconversion has been placed in the RF domain. There is of course nothing precluding also a TTD system to perform downconversion in the optical domain, either through a shifted and re-inserted carrier or the employment of frequency combs as shown in Figure 2c. In the case using a frequency comb, the downconversion happens via modulating the signal on one comb frequency line and subsequently detecting the beating between one of the sidebands and a different frequency line of the comb [30].

If only a single moving beam is needed, a simple corporate network structure is sufficient to realise the OBFN, such as in [31][32][33][34][35][36] using different PSs and TTD implementations. Figure 3 and 4 illustrate two potential solutions for extending the network to employ more simultaneous beams [12][29][37]. The blass matrix architecture is especially suited to the PAFR design since there will be little to no overlap in the beams. A blass matrix could be implemented with tunable couplers for each node in conjunction with phase shifters or tunable TTDs. Here, a ring resonator structure could be suitable if TTD is desired. Using a wavelength division multiplexing (WDM) strategy, as shown in Figure 4, would be more beneficial in a planar array antenna where each channel must be shared by every beam. Each beam would be dictated by the centre frequency of each tunable laser plus the RF carrier frequency giving a different TTD distribution across the different dispersive elements [38]. The several laser lines would all be multiplexed onto the same channel and distributed to the modulators, modulated, delayed according to the centre wavelengths and de-multiplexed before opto-electronic conversion. This type of solution requires a fast tunable laser with sufficiently high tuning speed while maintaining low RIN and linewidth, e.g. [39][40][41].

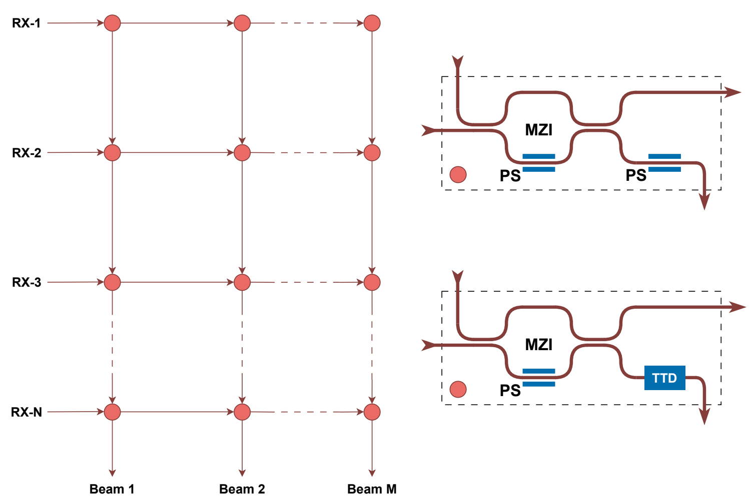

Figure 3: Optical blass matrix architecture. Each node consist of a tunable coupler and a PS or TTD.

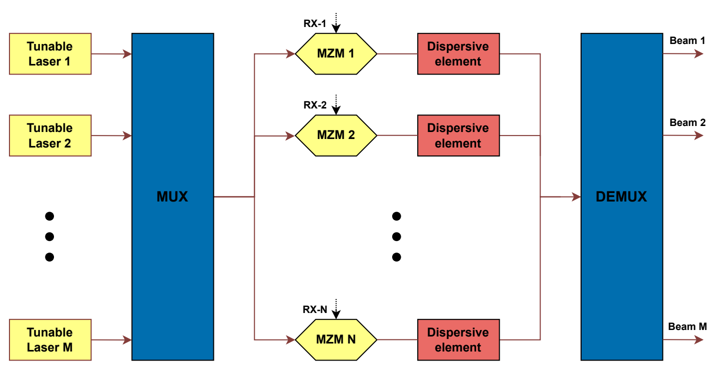

Figure 4: A TTD OBFN employing multiple tunable lasers, wavelength division multiplexing (WDM) and dispersive elements.

3.2. Material platforms

The feasibility of OBFNs in SAR systems hinges on the success and development of integrated microwave photonic technologies, such as Silicone-on-Insulator (SOI), Silicone Nitride (Si_3N_4), Indium Phosphide (InP), Lithium Niobate ($LiNbO_3$) and others [14]. These platforms are currently undergoing rapid development and are expected to reach sufficient maturation for SAR and many other areas in the near future [18][19].

Currently, assuming the optical C-band, there are two main material platforms potentially feasible for spaceborne SAR systems [14][15]. These are systems based on heterogeneous integration of either Silicon Photonics (SiPh) or Silicone Nitride (SiN) with other materials for the full spectrum of devices (amplifiers, lasers, detectors, modulators, filters, switches, delays, and/or phase shifters) [42]. This way the required functionalities can be employed without excessive propagation and interface losses. An overview of these materials and functions are listed in the following, with prominent materials for each function:

- Amplification and lasing
  - Indium Phosphide (InP)
- Modulation and Phase Shifting
  - Indium Phosphide (InP)
  - Lithium Niobate ($LiNbO_3$)
- Photodetection
  - Indium Phosphide (InP)
  - Germanium (Ge)

Functions such as coupling, switching and filtering can be realised through passive waveguide structures with modulators for tunability [43][44].

3.3. Optical Phase Shifters and TTD Elements

Optical phase shifters are an integral part of not only a phased array OBFN but also for tunable couplers, filters and many other functions. There are many ways of realising a phase shifter in IMWP. A selection of these, with their associated speeds, are;

- Thermal (TH) actuators (ca. 1 ms) [45]
- Piezoelectric (PZT) actuators (<1 µs) [46]
- Electro-optic modulators: [47]
  - Liquid Crystal (LC) actuators (<1 ms) [48]
  - Lithium Niobate on Insulator (LNOI) actuators (<1 ns) [49]
  - Indium Phosphide (or III-V) actuators (<1 ns) [50]

The reconfiguration speed of these actuators, whether they control TTD elements, phase shifters or couplers is primarily dependent on the chosen materials of the PIC element and secondarily dependent on the driving electronics.

There are several types of TTD elements prevalent in IMWP. These include photonic crystal waveguides, coupled microring resonators, waveguide bragg gratings, non-linear photonic solutions, and switchable delay lines [51]. The discussion on these solutions will not be significantly deep here. However, for SCORE SAR, the importance lies in solutions that can provide continuous or near continuous delay steps (as detailed in Table 1), have low losses and are fast enough for SCORE operation. Careful consideration of the dispersion variation across the RF bandwidth also need to be taken into account, since many delay methods offer a compact solution but a varying delay across the optical wavelength [51][52][53]. Structures using several microring resonators (MRR) often achieve a flat delay across a wide bandwidth with tunability via phase shifters in the rings and couplers. Many of these TTD methods exploit dispersive elements and are thus suitable for implementing structures such as those in Fig. 4, where the carrier wavelength is the tuned parameter.

3.4. Reconfiguration Speed

The dwell time of the first (and shortest) SCORE beam pointing direction, as shown in Table 3, puts a minimum speed required for potential PSs and TTDs implemented by a OBFN. In this case, the minimum speed is approximately at 1 MHz. However, given the assumption that the data acquired during beam weight reconfiguration is degraded or not useful at all, the speed needs to be a fraction of this limit. Table 4 lists the impact of the switching time on the loss, peak-sidelobe ratio (PSLR) and integrated sidelobe ratio (ISLR) respectively, assuming that the reconfiguration

Table 4: Impact on power loss, peak-sidelobe ratio (PSLR), and integrated sidelobe ratio (ISLR) for different photonic actuator switching speeds. Nominal PSLR and ISLR are -13.26 dB and -9.67 dB.

Switching time (ns) (% of dwell time)	Power loss (dB)	PSLR increase (dB)	ISLR increase (dB)
10 (1)	0.09	0.00	0.40
20 (2)	0.17	0.01	0.79
50 (5)	0.44	0.02	1.85
99 (10)	0.91	0.04	3.27
198 (20)	1.92	0.34	5.49
495 (50)	5.93	9.11	10.48

duration results in gaps in the acquired chirp. This reveals that the minimum speed required would lie somewhere less than 2 percent of the dwell time, that is >50 MHz in this case. That would restrict the viable solutions to electro-optic modulation techniques such as LNOI and InP from the previously listed materials. Given that LNOI PSs exhibit an exceptionally low loss this technology would be most suitable, despite the slightly larger footprint than InP solutions. Similarly, for a swept laser in conjunction with dispersive elements the exact wavelength error must fall within certain values in addition to the sweep speed being high enough, while noise performance does not degrade too much during the sweep compared to a static laser.

4. SYSTEM PERFORMANCE

4.1. Noise Performance

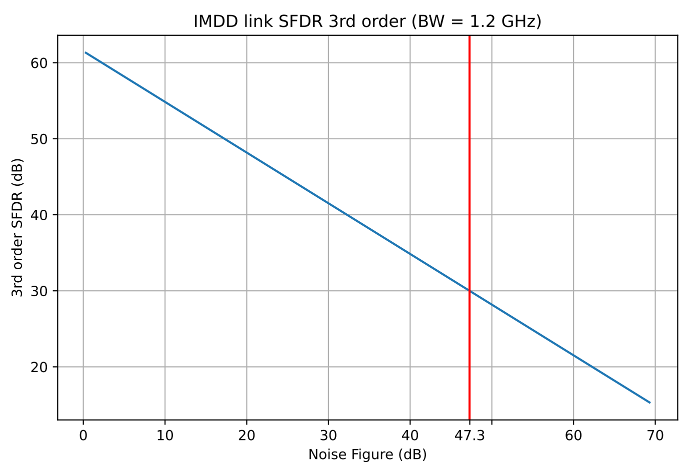

Figure 5: 3rd order spurious free dynamic range as a function of noise figure for a single channel optical link (1200 MHz bandwidth).

So far, the realisation of complex photonic networks and PICs have resulted in high noise figures of 30 dB or more. This is due to the high losses incurred in electro-optic conversion and the insertion loss of the many phase shift or time delay components required in a beamforming network [12][30]. These losses necessitate insertion of semiconductor optical amplifiers (SOA) that drive up the relative intensity noise (RIN) of the link. Ultimately, this requires extensive low noise amplification before insertion of the optical network. The noise factor trade-space of an analogue optical link is generally described by [54]

$$F = 1 + \frac{V_\pi^2}{\pi^2 R_i}\left(\frac{1}{I_{\rm dc}^2 R_o |H_{pd}|^2} + \frac{2q}{I_{\rm dc} k_B T_s} + \frac{\rm RIN}{k_B T_s}\right), \tag{2}$$

where V_π is the half-wave voltage of the modulator, R_i and R_o are input and output impedances of the optical link, $I_{\rm dc}$ is the average photocurrent produced in the photodiode, H_{pd} is the filter response of the photodiode, q is elemental charge, k_B is Boltzmann's constant, and T_s is the system temperature. The four terms present in (2) are, in order, the input thermal noise, output thermal noise, shot noise, and RIN, respectively. One of the most important sources of noise in a photonic system is the RIN of the laser. Additionally, for swept lasers, the RIN must remain sufficiently low during the sweep in addition to fixed operation. The most prevalent amplification material in PICs is InP, as previously discussed. These can now provide hundreds of milliwatts of power while maintaining low RIN in a small form factor [55], and are continuously improving as the technology matures, but there are also alternative amplification methods being developed, such as the erbium-doped waveguide amplifier (EDWA) [56]. In this recent development SiN has been successfully doped by erbium and exhibits similar performance to the erbium-doped fibre amplifiers, which revolutionised the fibre-optic communications industry.

4.2. Dynamic Range

The single most impacting effect on the optical link dynamic range for single octave systems is the 3rd order spurious-free dynamic range (SFDR_3). The trade-space is described by [54]

$$\mathrm{SFDR}_3 = \left(\frac{4V_\pi^2}{\pi^2 R_i k_B T_s B}\right)^{2/3} \left(\frac{1}{F}\right)^{2/3}. \tag{3}$$

The maximum possible bandwidth that can be utilized by a spaceborne SAR is dictated by the ITU regulations for frequency allocation, and is currently placed at X-band with 1200 MHz bandwidth [25]. Given this limitation and an assumed $V_\pi = 1V$, $R_i = 50\Omega$, $T_s = 290K$, the SFRD_3 can be plotted vs. NF, as seen in Fig. 5. The SAR required dynamic range of 30 dB, given in Table 1, would then be satisfied as long as the NF is below ca. 45 dB. Given this generous limitation, it can be concluded that the major limiting factor for an optical link implemented in SAR is achieving a certain system NF and thereby the required NESZ fulfilling the sensitivity requirements.

5. DISCUSSION AND CONCLUSION

The goal is to implement a high performance analogue photonic link with an OBFN and possible downconversion of the RF signal in the optical domain, while also improving the SWaP. Therefore, the current state-of-the-art and near future trends in analogue microwave photonics suggest that a heterogeneous integration of many materials in a PIC platform is optimal. The lowest loss waveguide is currently occupied by the SiN technology, while the lowest loss modulators and phase shifters, with sufficient speed, are LNOI. The most appropriate low-noise high-power single frequency laser would be an external laser or InP integrated laser. SOA should be minimized as far as possible to keep the NF low, but should it be required, InP amplifiers are the current best alternative. This is potentially surpassed in the near future by the development of EDWA, best employed as amplifiers right after electro-optic modulation or right before photodetection.

The current PIC capabilities indicate a lower number of channels, and as such a PAFR or PA sub-array architecture would serve as an initial implementation. The numbers used in this work are very strict and could be relaxed in order to realize a simpler SAR system. For example, the number of pointing directions for each SCORE beam could be reduced and allow for slower PSs using PZT or TH actuators. Another obvious relaxation is the reduction of the number of channels to reduce the complexity. Finally, the rapid, Moore's Law like, development of the integrated photonics sector indicate that the limitation of number of components and channels will quickly diminish over time, enabling the use of large phased arrays using IMWP technology.

REFERENCES

1. A. Freeman *et al.*, "The "myth" of the minimum SAR antenna area constraint," *IEEE Trans. Geosci. Remote Sens.*, vol. 38, pp. 320–324, Jan. 2000.
2. J. C. Curlander and R. N. McDounough, *Synthetic Aperture Radar: Systems and Signal Processing*, 1st ed. New York, USA: John Wiley and Sons Inc., 1991.
3. J. H. Blythe, "Radar systems," U.S. Patent 4 253 098, Feb., 1981.
4. J. T. Kare, "Moving receive beam method and apparatus for synthetic aperture radar," U.S. Patent US 6 175 326, Jan. 16, 2001. [Online]. Available: https://www.osti.gov/biblio/873501
5. M. Süß and W. Wiesbeck, "Side-looking synthetic aperture radar," European Patent Patent EP 1 241 487, Sep., 2002.
6. G. Krieger, N. Gerbert, M. Younis, F. Bordoni, and A. Moreira, "Advanced concepts for ultra-wide-swath SAR imaging," in *7th European Conf. on Synthetic Aperture Radar*, Friedrichshafen, Germany, Jun. 2008.

7. A. Freeman, G. Krieger, P. Rosen, M. Younis, W. T. K. Johnson, R. Jordan, and A. Moreira, "Sweep-SAR: Beam-forming on receive using a reflector-phased array feed combination for spaceborne SAR," in *IEEE National Radar Conference*, Jun. 2009.
8. S. Huber, M. Younis, A. Patyuchenko, G. Krieger, and A. Moreira, "Spaceborne reflector SAR systems with digital beamforming," *IEEE Trans. Aerosp. Electron. Syst.*, vol. 48, pp. 3473–3493, Oct. 2012.
9. M. Villano, G. Krieger, and A. Moreira, "Staggered SAR: High-resolution wide-swath imaging by continuous PRI variation," *IEEE Trans. Geosci. Remote Sens.*, vol. 52, pp. 4462–4479, Nov. 2013.
10. J. Capmany and D. Novak, "Microwave photonics combines two worlds," *Nature Photonics*, vol. 1, pp. 319–330, Jun. 2007.
11. R. A. Minasian, "Ultra-wideband and adaptive photonic signal processing of microwave signals," *IEEE J. Quantum Electron.*, vol. 52, Jan. 2016.
12. M. Reza *et al.*, "Design and performance estimation of a photonic integrated beamforming receiver for scan-on-receive synthetic aperture radar," *J. Lightw. Technol.*, vol. 39, pp. 7588–7599, Dec. 2021.
13. G. Serafino *et al.*, "Toward a new generation of radar systems based on microwave photonic technologies," *J. Lightw. Technol.*, vol. 37, Jan. 2019.
14. D. Marpaung, J. Yao, and J. Capmany, "Integrated microwave photonics," *Nature photonics*, vol. 13, no. 2, pp. 80–90, 2019.
15. S. Iezekiel, M. Burla, J. Klamkin, D. Marpuang, and J. Capmany, "RF engineering meets optoelectronics: Progress in integrated microwave photonics," *IEEE Microw. Mag.*, vol. 16, pp. 28–45, Sep. 2015.
16. M. Krainak *et al.*, "Integrated photonics for NASA applications," in *SPIE LASE*, San Fransisco, California, USA, Feb. 2019.
17. M. Smit, J. van der Tol, and M. Hill, "Moore's law in photonics," *Lasers & Photonics Reviews*, vol. 6, Jan. 2012.
18. M. Smit *et al.*, "An introduction to InP-based generic integration technology," *Semiconductor Science and Technology*, vol. 29, Jun. 2014.
19. M. J. R. Heck, "The road ahead for integrated photonics (tutorial)," in *IEEE Photonics Conference (IPC)*, Vancouver, BC, Canada, Nov. 2022.
20. F. Queiroz de Almeida, T. Rommel, M. Younis, G. Krieger, and A. Moreira, "Multichannel staggered SAR: System concepts with reflector and planar antennas," *IEEE Trans. Aerosp. Electron. Syst.*, vol. 55, pp. 877–902, Apr. 2019.
21. F. T. Ulaby, M. C. Dobson, and J. L. Álvarez Pérez, *Handbook of Radar Scattering Statistics for Terrain*, 2nd ed. Boston, MA, USA: Artech House, 2019.
22. H. L. V. Trees, *Optimum Array Processing: Part IV of Detection, Estimation, and Modulation Theory*, 1st ed. New York, USA: John Wiley & Sons, Inc., 2002.
23. R. Kinsey, "Phased array beam spoiling technique," *IEEE Antennas and Propagation Society International Symposium*, vol. 2, pp. 698–701, 1997.
24. R. Düring, F. N. Koudogbo, and M. Weber, "TerraSAR-X and TanDEM-X: Revolution in spaceborne radar," *Int. Arch. Photogramm. Remote Sens. Spat. Inf. Sci*, vol. 37, pp. 227–234, 2008.
25. *Radio Regulations - Articles.* International Telecommunications Union (ITU), 2020, vol. 1, ch. 2.
26. S. Huber, M. Younis, G. Krieger, and A. Moreira, "Error analysis for digital beamforming synthetic aperture radars: A comparison of phased array and array-fed reflector systems," *IEEE Trans. Geosci. Remote Sens.*, vol. 59, pp. 6314–6322, Aug. 2021.
27. R. J. Mailloux, *Phased Array Antenna Handbook*, 3rd ed. Norwood, USA: Artech House, 2018.
28. S. Huber, M. Younis, G. Krieger, A. Moreira, and W. Wiesbeck, "A reflector antenna concept robust against feed failures for satellite communications," *IEEE Trans. Antennas Propag.*, vol. 63, pp. 1218–1224, Apr. 2015.
29. C. Tsokos *et al.*, "Analysis of a multibeam optical beamforming network based on blass matrix architecture," *J. Lightw. Technol.*, vol. 36, pp. 3354–3372, Aug. 2018.
30. M. Reza *et al.*, "Multi-static multi-band synthetic aperture radar (SAR) constellation based on integrated photonic circuits," *Electronics*, vol. 11, 2022.
31. K. Entesari, S. Palermo, C. Madsen, G. Choo, S. Cai, and B. Wang, "Silicon photonics for microwave applications," *IEEE Microw. Mag.*, vol. 21, pp. 20–42, Aug. 2020.
32. A. Meijerink *et al.*, "Novel ring resonator-based integrated photonic beamformer for broadband phased array receive antennas—part I: Design and performance analysis," *J. Lightw. Technol.*, vol. 28, no. 1, pp. 3–18, Jan. 2010.

33. L. Zhuang *et al.*, "Novel ring resonator-based integrated photonic beamformer for broadband phased array receive antennas—part II: Experimental prototype," *J. Lightw. Technol.*, vol. 28, no. 1, pp. 19–31, Jan. 2010.
34. H. Sun *et al.*, "Broadband 1x8 optical beamforming network based on anti-resonant microring delay lines," *J. Lightw. Technol.*, vol. 40, no. 10, Oct. 2022.
35. C. Tsokos *et al.*, "True time delay optical beamforming network based on hybrid InP-silicon nitride integration," *J. Lightw. Technol.*, vol. 39, pp. 5845–5854, Sep. 2021.
36. C. Zhu *et al.*, "Silicon integrated microwave photonic beamformer," *Optica*, vol. 7, no. 9, pp. 1162–1170, Sep. 2020.
37. C. G. H. Roeloffzen *et al.*, "Integrated optical beamformers," in *Optical Fiber Communication Conference*. Optica Publishing Group, Dec. 2015.
38. C. Wang and J. Yao, *Microwave Photonics.* Boca Raton, Florida: CRC Press, 2013, ch. 4.
39. S. Dhoore, G. Roelkens, and G. Morthier, "Fast wavelength-tunable lasers on silicon," *IEEE Journal of Selected Topics in Quantum Electronics*, vol. 25, 11 2019.
40. V. Snigirev *et al.*, "Ultrafast tunable lasers using lithium niobate integrated photonics," *Nature*, vol. 615, pp. 411–417, 3 2023.
41. Z. Sun *et al.*, "Tunable laser via high-density integration of DFB lasers with high precision wavelength spacings," *IEEE Photonics Technology Letters*, vol. 34, pp. 467–470, 5 2022.
42. S. Yegnanarayanan *et al.*, "Integrated microwave photonic subsystems," in *IEEE Research and Applications of Photonics in Defense Conference (RAPID)*, Miramar Beach, Florida, USA, Aug. 2020.
43. J. Capmany and D. Novak, "A tutorial on microwave photonics filters," *J. Lightw. Technol.*, vol. 24, pp. 201–229, Jan. 2006.
44. Y. Liu, A. Choudhary, D. Marpaung, and B. J. Eggleton, "Integrated microwave photonic filters," *Advances in Optics and Photonics*, vol. 12, no. 6, pp. 487–555, 2020.
45. D. Pérez *et al.*, "Thermal tuners on a silicon nitride platform," *arXiv preprint arXiv:1604.02958*, 2016.
46. J. P. Epping, D. Marchenko, A. Leinse, R. Mateman, M. Hoekman, L. Wevers, E. J. Klein, C. G. Roeloffzen, M. Dekkers, and R. G. Heideman, "Ultra-low-power stress-optics modulator for microwave photonics," in *Integrated Optics: Devices, Materials, and Technologies XXI*, vol. 10106. SPIE, 2017, pp. 80–87.
47. G. Sinatkas, T. Christopoulos, O. Tsilipakos, and E. E. Kriezis, "Electro-optic modulation in integrated photonics," *Journal of Applied Physics*, vol. 130, Jul. 2021.
48. K. Wörhoff, A. Ryabchun, M. Hoekman, J. Epping, R. Grootjans, and A. Leinse, "Liquid crystal phase modulator integration on the TriPleX photonic platform," in *International Conference on Space Optics (ICSO)*, Chania, Greece, Oct. 2018.
49. M. Zhang, C. Wang, P. Kharel, D. Zhu, and M. Lončar, "Integrated lithium niobate electro-optic modulators: when performance meets scalability," *Optica*, vol. 8, pp. 652–667, May 2021.
50. Y. Jiao and other, "InP membrane integrated photonics research," *Semiconductor Science and Technology*, vol. 36, no. 1, dec 2020. [Online]. Available: https://dx.doi.org/10.1088/1361-6641/abcadd
51. B. Paul, K. Sertel, and N. K. Nahar, "Photonic beamforming for 5G and beyond: A review of true time delay devices enabling ultra-wideband beamforming for mmWave communications," *IEEE Access*, vol. 10, pp. 75 513–75 526, 2022.
52. W. Shi, V. Veerasubramanian, D. Patel, and D. V. Plant, "Tunable nanophotonic delay lines using linearly chirped contradirectional couplers with uniform bragg gratings," *Optics Letters*, vol. 39, no. 3, pp. 701–703, Feb. 2014.
53. I. Giuntoni, D. Stolarek, D. I. Kroushkov, J. Bruns, L. Zimmermann, B. Tillack, and K. Petermann, "Continuously tunable delay line based on SOI tapered Bragg gratings," *Optics Express*, vol. 20, no. 10, pp. 11 241–11 246, May 2012. [Online]. Available: https://opg.optica.org/oe/abstract.cfm?URI=oe-20-10-11241
54. V. J. Urick, J. D. Mckinney, and K. J. Williams, *Fundamentals of Microwave Photonics*, 1st ed. Hoboken, New Jersey: John Wiley and Sons Inc., 2015.
55. D. Kharas *et al.*, "High-power (>300 mW) on-chip laser with passively aligned silicon-nitride waveguide DBR cavity," *IEEE Photonics Journal*, vol. 12, 1 2020.
56. Y. Liu *et al.*, "A photonic integrated circuit-based erbium-doped amplifier," *Science*, vol. 376, no. 6599, pp. 1309–1313, 2022.